ADVANCED ENERGY MATERIALS
www.advenergymat.de

Bandgap Narrowing in Non-Fullerene Acceptors: Single Atom Substitution Leads to High Optoelectronic Response Beyond 1000 nm

Jaewon Lee, Seo-Jin Ko, Martin Seifrid, Hansol Lee, Benjamin R. Luginbuhl, Akchheta Karki, Michael Ford, Katie Rosenthal, Kilwon Cho, Thuc-Quyen Nguyen,* and Guillermo C. Bazan**

Two narrow bandgap non-fullerene acceptors (NBG-NFAs), namely, COTIC-4F and SiOTIC-4F, are designed and synthesized for the fabrication of efficient near-infrared organic solar cells (OSCs). The chemical structures of the NBG-NFAs contain a D′-D-D′ electron-rich internal core based on a cyclopentadithiophene (or dithienosilole) (D) and alkoxythienyl (D′) core, end-capped with the highly electron-deficient unit 2-(5,6-difluoro-3-oxo-2,3-dihydro-1H-inden-1-ylidene)malononitrile (A), ultimately providing a A-D′-D-D′-A molecular configuration that enhances the intramolecular charge transfer characteristics of the excited states. One can thereby reduce the optical bandgap (E_g^{opt}) to as low as ≈1.10 eV, one of the smallest values for NFAs reported to date. In bulk-heterojunction (BHJ) OSCs, NBG-NFA blends with the polymer donor PTB7-Th yield power conversion efficiencies (PCE) of up to 9.0%, which is particularly high when compared against a range of NBG BHJ blends. Most significantly, it is found that, despite the small energy loss ($E_g^{opt} - eV_{OC}$) of 0.52 eV, the PTB7-Th/NBG-NFA bulk heterojunction blends can yield short-circuit current densities of up to 22.8 mA cm^{-2}, suggesting that the design and application of NBG-NFA materials have substantial potential to further improve the PCE of OSCs.

Near-infrared (NIR) organic semiconductors have attracted interest due to their relevance for enabling efficient semitransparent organic solar cells (OSCs).[1–3] Ideally, such materials should strongly absorb light in the NIR region of the spectrum, while remaining transparent in the visible region.[4,5] Several polymeric and small molecular donor materials with absorption spectra extending to the NIR region have been designed and applied to the fabrication of OSCs.[6–8] A critical challenge arises as one decreases optical bandgaps (E_g^{opt}) with respect to simultaneously achieving a high external quantum efficiency (EQE) and high open-circuit voltage (V_{OC}).[9] This challenge is due to the counterbalance between the driving force for charge separation, which aids in photocurrent generation, and voltage loss in the cell.[10,11] Finding ways to maximize V_{OC} requires one to reduce the energy loss ($E_{loss} = E_g^{opt} - eV_{OC}$) that occurs as a result of the multiple states that follow exciton generation.[12]

Narrow bandgap (NBG) non-fullerene acceptors (NFAs) have emerged as the next generation of electron acceptors in OSCs.[13–18] Tunability of E_g^{opt} through molecular design allows one to tailor NIR absorption characteristics.[19,20] Considering that the maximum human photopic sensitivity is 555 nm and the maximum human scotopic sensitivity is 507 nm,[21] transparent photoactive materials should predominantly absorb solar radiation from ≈650 nm into the NIR region for semitransparent solar cell applications. In addition, since ≈50% of solar radiation intensity is in the NIR region, the development of NBG-NFAs with E_g^{opt} below ≈1.35 eV is desirable to effectively harvest solar NIR radiation.[1] Another encouraging feature of NFAs is that the energetic offsets that drive charge generation are small (<0.3 eV),[18,22–24] which is beneficial for maintaining low E_{loss}. Despite these desirable features, there has been less consideration for designing NBG-NFAs for transparent/NIR absorbing OSC applications. To address this challenge and expand the design of NIR harvesting acceptor molecules, we demonstrate in this contribution a new molecular design for ultra NBG-NFA materials with strong NIR response and small E_{loss}.

The two NBG NFAs described in this contribution are COTIC-4F and SiOTIC-4F (**Figure 1**a). Their molecular design includes incorporation of a cyclopentadithiophene (CPDT), or dithienosilole (DTS), unit as the central donor (D) fragment, which is flanked by two alkoxythienyl units (D′) to form an electron-rich D′-D-D′ central core. The D′-D-D′ units are end-capped with

Dr. J. Lee, Dr. S.-J. Ko, M. Seifrid, B. R. Luginbuhl, A. Karki, M. Ford, K. Rosenthal, Prof. T.-Q. Nguyen, Prof. G. C. Bazan
Center for Polymers and Organic Solids
Department of Chemistry and Department of Biochemistry
University of California at Santa Barbara
Santa Barbara, CA 93106, USA
E-mail: quyen@chem.ucsb.edu; bazan@chem.ucsb.edu
H. Lee, Prof. K. Cho
Center for Advanced Soft Electronics
Department of Chemical Engineering
Pohang University of Science and Technology
Pohang 37673, Korea
E-mail: kwcho@postech.ac.kr
The ORCID identification number(s) for the author(s) of this article can be found under https://doi.org/10.1002/aenm.201801212.

DOI: 10.1002/aenm.201801212

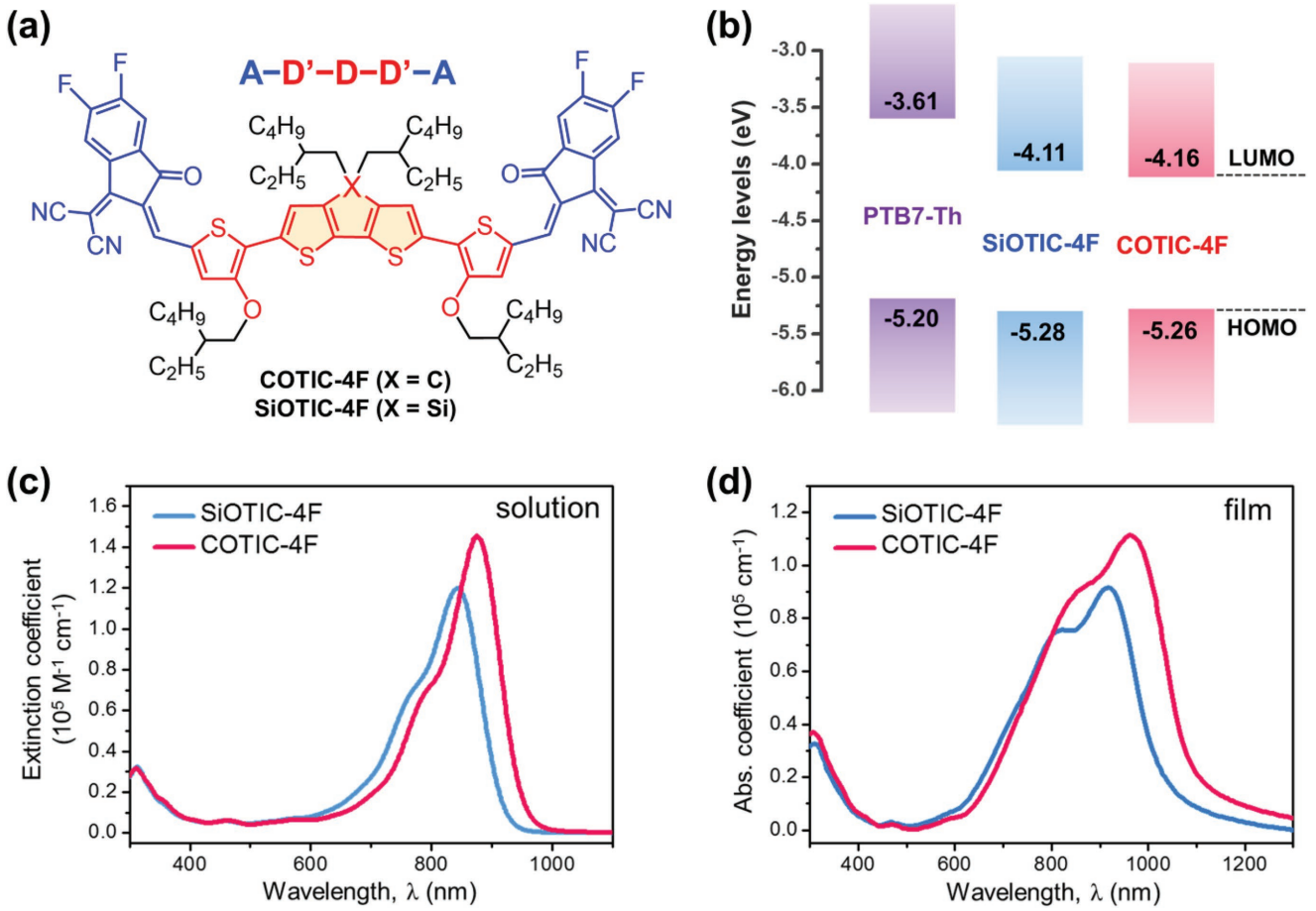

Figure 1. a) Molecular structures of COTIC-4F and SiOTIC-4F. b) Energy level diagram of PTB7-Th, SiOTIC-4F, and COTIC-4F. HOMO levels were obtained from film CV measurements. LUMO levels calculated by the following equation: $E_{LUMO} = E_g^{opt} + E_{HOMO}$. c,d) UV–vis–NIR absorption spectra of COTIC-4F and SiOTIC-4F in chloroform solution and as a thin solid film.

the electron-deficient (A) unit 2-(5,6-difluoro-3-oxo-2,3-dihydro-1H-inden-1-ylidene)malononitrile, ultimately providing a A-D′-D-D′-A molecular configuration with the proper attributes to achieve the target intramolecular charge transfer (ICT) effect.[25] At the most elementary view, the E_{loss} can be reduced by minimizing the energetic offset between the highest occupied molecular orbital (HOMO) levels of the donor and acceptor components in the active layer ($HOMO_D$–$HOMO_A$, ΔE_{HOMO}), while providing a sufficient driving force for charge separation.[19,23] Combining strong electron-donating D and D′ subunits in the D′-D-D′ configuration was anticipated to raise the HOMO levels of resulting molecules, with the intent of minimizing ΔE_{HOMO}. Our molecular design thus aims to provide targets molecules with a narrow E_g^{opt} while concomitantly reducing E_{loss}. Additional design considerations include the presence of conformational "locks" via S···O interactions involving proximate alkoxy groups and thienyl S atoms to favor coplanarity of the overall π-conjugated system and thus decrease the localized π–π* transition in the high-energy wavelengths.[26–28] Moreover, the alkoxy groups are essential to ensure sufficient solubility for the fabrication of device using solution deposition. Finally, fluorination of the end-capping moieties further enhances the ICT effect, thereby yielding narrower bandgaps than the nonfluorinated analogues.[29,30] Indeed, COTIC-4F and SiOTIC-4F exhibit strong NIR absorption with narrow E_g^{opt} of 1.10 and 1.17 eV, respectively. To the best of our knowledge, the E_g^{opt} of 1.10 eV is the lowest value for NFA small molecule acceptors reported thus far.

Scheme S1 (Supporting Information) shows the synthetic route of COTIC-4F and SiOTIC-4F by means of two facile reactions. Stille coupling reaction between (4,4′-di-2-ethylhexyl-4H-cyclopenta[1,2-b:5,4-b′]dithiophene-2,6-diyl)bis(trimethylstanne) (1) and 5-bromo-4-((2-ethylhexyl)oxy)thiophene-2-carbaldehyde (3) in the presence of catalytic $Pd(PPh_3)_4$ in anhydrous toluene produced dialdehyde 4. Subsequently, Knoevenagel condensation reaction between compound 4 and 2-(5,6-difluoro-3-oxo-2,3-dihydro-1H-inden-1-ylidene)malononitrile (6) afforded COTIC-4F in 78% yield as a dark-green solid. Similar synthetic strategies and reaction conditions were used to prepare SiOTIC-4F in 75% yield. The new compounds were fully characterized by spectroscopic methods (see the Supporting Information). COTIC-4F and SiOTIC-4F exhibit good solubility in common organic solvents such as dichloromethane, chloroform (CF), and chlorobenzene (CB) at room temperature, and good thermal stability with decomposition temperatures (T_d, 5% weight loss) of 328 and 368 °C for COTIC-4F and SiOTIC-4F, respectively, as measured using thermogravimetric analysis (Figure S5, Supporting Information).

Cyclic voltammetry (CV) measurements were carried out in order to estimate orbital energy levels (Figure S6, Supporting Information). The HOMO and LUMO levels were deduced from the onsets of the oxidation and reduction peaks. These estimates provided $HOMO_{CV}$ levels of COTIC-4F and SiOTIC-4F of −5.26 ± 0.05 and −5.28 ± 0.05 eV, respectively. We must recognize that the E_{HOMO} values are within experimental error relative to each other and that CV-determined values are different from what may be expected in the neat state (i.e., without supporting electrolyte) or in blends.[31] From the reduction onsets, the $LUMO_{CV}$ levels were measured to be −4.17 and −4.12 eV for COTIC-4F and SiOTIC-4F, respectively. LUMO levels calculated by the following equation: $E_{LUMO} = E_g^{opt} + E_{HOMO}$ are −4.16 and −4.11 eV for COTIC-4F and SiOTIC-4F, respectively, which are similar to the values calculated from the CV measurements. By and large, state-of-the-art NFA small molecules have acceptor-donor-acceptor (A-D-A) molecular structures with HOMO levels in the range of −5.4 to −5.6 eV.[19,20] COTIC-4F and SiOTIC-4F thus possess higher HOMO levels relative to more conventional A-D-A NFAs, which is desirable for mitigating energy losses. In addition, because most reported narrow bandgap polymer donors (NBG-PDs) exhibit HOMO levels below −5.2 ± 0.1 eV, COTIC-4F and SiOTIC-4F offer opportunities for pairing with a variety of NBG-PDs.

Absorption spectra of solutions of SiOTIC-4F and COTIC-4F are shown in Figure 1c. In CF solution, COTIC-4F displays absorption in the 750–950 nm region with an absorption maximum (λ_{max}) at 875 nm. SiOTIC-4F displays similar features in solution, however there is an ≈33 nm blueshift in the general features, relative to COTIC-4F. As shown in Figure 1d, the absorption of the films exhibits a redshift (≈100 nm) compared to what is observed in solution. Optical transitions of both NFA molecules are located in the NIR region, with small E_g^{opt} of 1.10 and 1.17 eV for COTIC-4F and SiOTIC-4F, respectively.

Theoretical calculations were performed at the density functional (DFT) level of theory with the semiempirically tuned ωB97XD/6-31G (d,p) functional and basis set to understand the influence of the bridging atom on the electronic structures and molecular conformations of COTIC-4F and SiOTIC-4F.[32,33] As illustrated in Figure S7 (Supporting Information), the HOMO electron densities are mainly localized around the central donor complexes (D′-D-D′) including the dicyanomethylidene and carbonyl groups on the end-dye units, while the LUMO electron density is distributed throughout the whole conjugated backbone. The HOMO/LUMO energy levels are calculated to be −5.04 eV/−3.35 eV and −5.09 eV/−3.34 eV for COTIC-4F and SiOTIC-4F, respectively (Figure S7, Supporting Information), which agrees with the trend observed in the experimental results. Time-dependent DFT calculations performed in a chloroform dielectric using the conductor-like polarizable continuum model also fit well with the solution absorption spectra (Figure S8, Supporting Information). One possible explanation for the bandgap modulation may be the difference in bond lengths resulting from the change in bridging atom. The longer Si−C_3 bond (≈1.90 Å) of DTS (Figure S9, Supporting Information), compared to the C−C_3 bond (≈1.53 Å), pushes out the flanking thiophene rings. This results in a lengthening of the C−C bond linking the two thiophene rings: 1.43 Å for CPDT versus 1.45 Å for DTS (Table S2, Supporting Information). The shorter C−C bond linking the two thiophene rings in the CPDT unit favors a larger quinoidal character in COTIC-4F than in SiOTIC-4F, which in turn narrows the bandgap of COTIC-4F versus SiOTIC-4F. It is worth pointing out that several examples in the literature indicate a stronger donor quality to CPDT versus DTS.[34–37] The optimized geometries of both NFAs feature planar backbones and high symmetry with a "zigzag"-type conformation (Figure S10, Supporting Information).

To evaluate the performance of SiOTIC-4F and COTIC-4F, solar cells were fabricated with the architecture ITO/ZnO/PTB7-Th:NFA/MoO_3/Ag. The widely used PTB7-Th polymer was chosen as the electron donor to pair with COTIC-4F and SiOTIC-4F based on the following considerations. First, the HOMO level (−5.20 eV) of PTB7-Th is close to the HOMO levels of the acceptors (Figure 1b), which is beneficial to minimize charge transfer energy losses. Second, PTB7-Th shows complementary absorption properties with those of COTIC-4F or SiOTIC-4F, so that the PTB7-Th:NFA films absorb across a broad region of solar radiation from 500 to 1100 nm (Figure S11, Supporting Information).

Device fabrication conditions, such as the PTB7-Th:NFA weight ratio and processing solvent were varied to determine the optimal conditions (Figure S12 and Table S3, Supporting Information). The best performance was obtained at a 1:1.5 PTB7-Th:NFA ratio spin-coated from CB with 2 vol% 1-chloronaphthalene (CN) for COTIC-4F and CF with 2 vol% CN for SiOTIC-4F. After optimizing the device fabrication conditions, a PCE of 9.0% with a remarkably high J_{SC} of 22.8 mA cm^{-2} was obtained for the best PTB7-Th:SiOTIC-4F-based device, which is higher than that of the PTB7-Th:COTIC-4F-based counterpart (PCE = 7.4%). **Figure 2**a shows the current density–voltage (*J*–*V*) curves and **Table 1** summarizes relevant photovoltaic parameters of the optimized OSC devices. Note that the difference in V_{OC} between the two optimal devices is close to the $\triangle E_{LUMO}$ of COTIC-4F versus SiOTIC-4F (≈0.05 eV).

EQE spectra of the optimized devices are shown in Figure 2b. One observes broad spectral response in the 300–1050 nm region for SiOTIC-4F and 300–1150 nm for COTIC-4F, indicating that both the NFA and PTB7-Th components contribute to the J_{SC}. The EQE of PTB7-Th:SiOTIC-4F is above 55% in the range of 550–900 nm, with the maximum value approaching 70% at 610 nm. This result indicates that despite a very small ΔE_{HOMO} (<0.1 ± 0.05 eV) efficient hole transfer from the NFA to PTB7-Th occurs. We reiterate that the energetic offset calculated from the CV are known to be rough estimates, therefore we make these comments with caution. The calculated J_{SC} extracted from the EQE spectra corresponds well with the values from *J*–*V* curves within ≈5% deviation. The PTB7-Th:SiOTIC-4F-based optimized devices exhibited an average V_{OC} of 0.65 V, indicating that the E_{loss} is estimated to be ≈0.52 eV. The average visible transmittances (AVT, 370–740 nm) of the ITO glass/ZnO/BHJ films are 53 and 49% for SiOTIC-4F and COTIC-4F, respectively (Figure S13, Supporting Information). Thus, SiOTIC-4F and COTIC-4F have potential as components for semitransparent OSC applications. Charge carrier transport was examined using hole- and electron-only devices

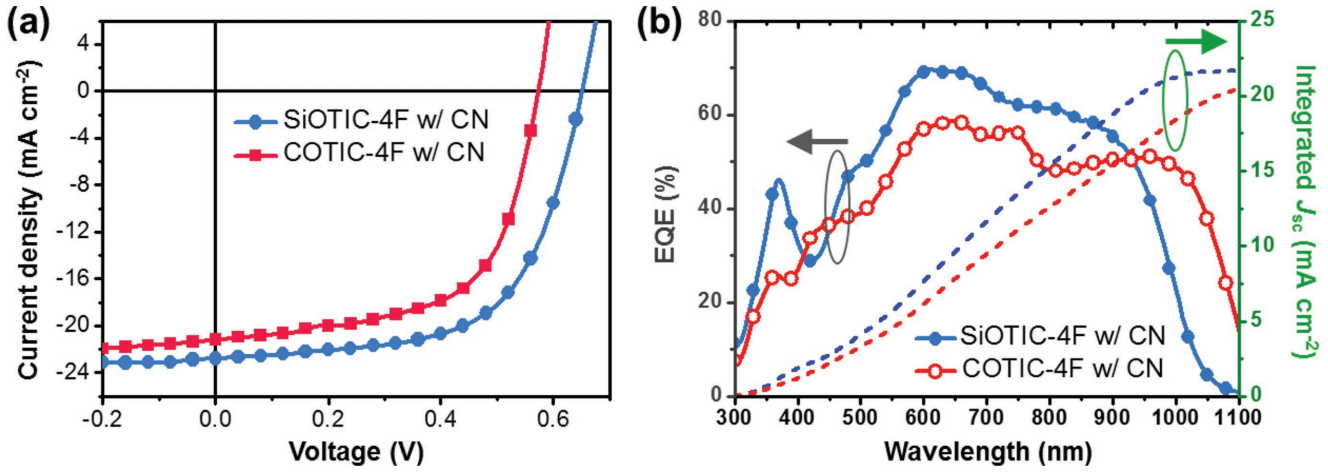

Figure 2. a) *J–V* characteristics and b) EQE spectra and corresponding curves integrated from the EQE data of the optimized OSC devices blended with PTB7-Th under illumination of an AM 1.5 G at 100 mW cm^{-2}.

Table 1. Performance of OSCs based on PTB7-Th:NFAs blends.

Blends[a)]	V_{OC} [V]	J_{SC} [mA cm^{-2}]	FF [%]	PCE$_{ave\ (max)}$[b)] [%]
SiOTIC-4F	0.65 ± 0.01	21.6 ± 1.0	61.4 ± 3.7	8.6 ± 0.2 (9.0)
COTIC-4F	0.56 ± 0.01	20.3 ± 1.2	56.3 ± 4.2	6.4 ± 0.8 (7.4)

[a)]PTB7-Th:NFA ratio is 1:1.5 (w/w). Processing solvents for SiOTIC-4F and COTIC-4F are CF:2%CN and CB:2%CN, respectively; [b)]Average values from 15 devices.

(Figure S14 and Table S5, Supporting Information). Using the space charge-limited current (SCLC) method, the hole and electron mobilities of PTB7-Th:SiOTIC-4F were estimated to be 3.3×10^{-4} and 9.8×10^{-5} cm^2 V^{-1} s^{-1}, respectively. The balanced hole/electron mobilities in the blend film are beneficial for reducing space charge accumulation and thus facilitating charge extraction.

Topographic and photoresponsive features were also examined by using the photoconductive atomic force microscopy (pc-AFM) technique.[38–40] As displayed in **Figure 3**a,b, the AFM height images indicate that both the SiOTIC-4F- and COTIC-4F-based films have smooth surface features with comparable root-mean-square roughness of 1.7 and 2.2 nm, respectively. Using pc-AFM, along with the height image, a current image can also be obtained which provides information about the size of the photoconductive domains (Figure 3c,d). Current scans in Figure 3c,d suggest that both blends have a finely mixed morphology and a clear phase separation between the donor and acceptor domains cannot be visualized. Interestingly, the SiOTIC-4F blend has an overall larger current magnitude than the COTIC-4F blend, corroborating the measured J_{SC} values. Transmission electron microscopy (TEM) measurements (Figure S15, Supporting Information) also showed that the blend films for both NFAs have comparable morphological properties.

Grazing incidence wide-angle X-ray scattering (GIWAXS) was employed to investigate the crystalline features of the thin films. The 2D GIWAXS patterns with the line-cut profiles are summarized in Figures S16–S18 (Supporting Information), and the corresponding crystallographic information summarized in Tables S6 and S7 (Supporting Information). First, the single-component thin films were measured using the same processing solvents as the optimized OSC devices (Figure S16, Supporting Information). The intense (100) diffraction peak (q_z = 0.41 Å^{-1}) of the as-spun COTIC-4F is dominantly observed, indicating that the texture adopts edge-on crystallites with respect to the substrate.[41] On the contrary, the as-spun SiOTIC-4F tends to adopt a face-on orientation with a high-intensity

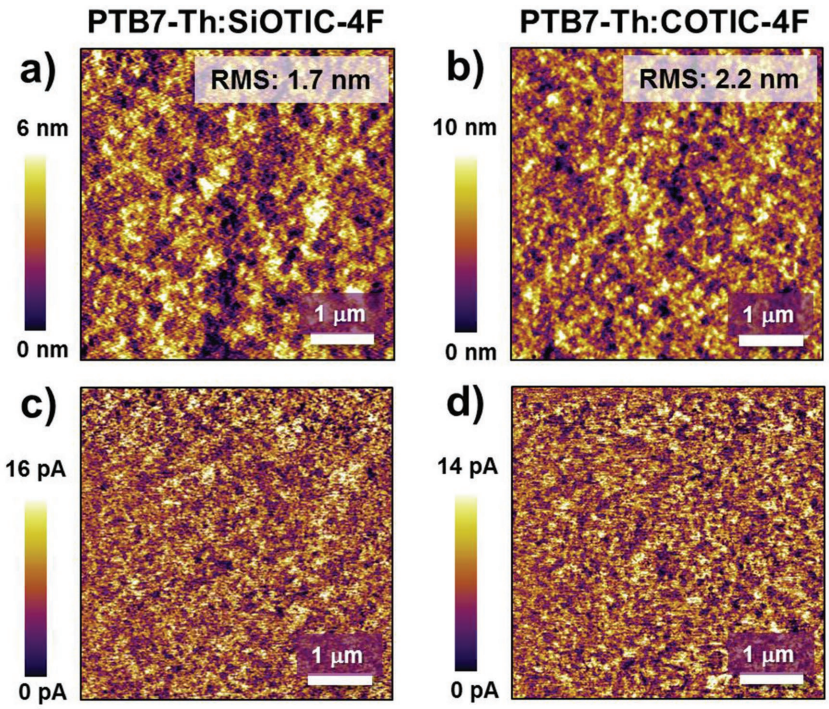

Figure 3. a,b) AFM height images and c,d) photoconductive AFM images of blend films.

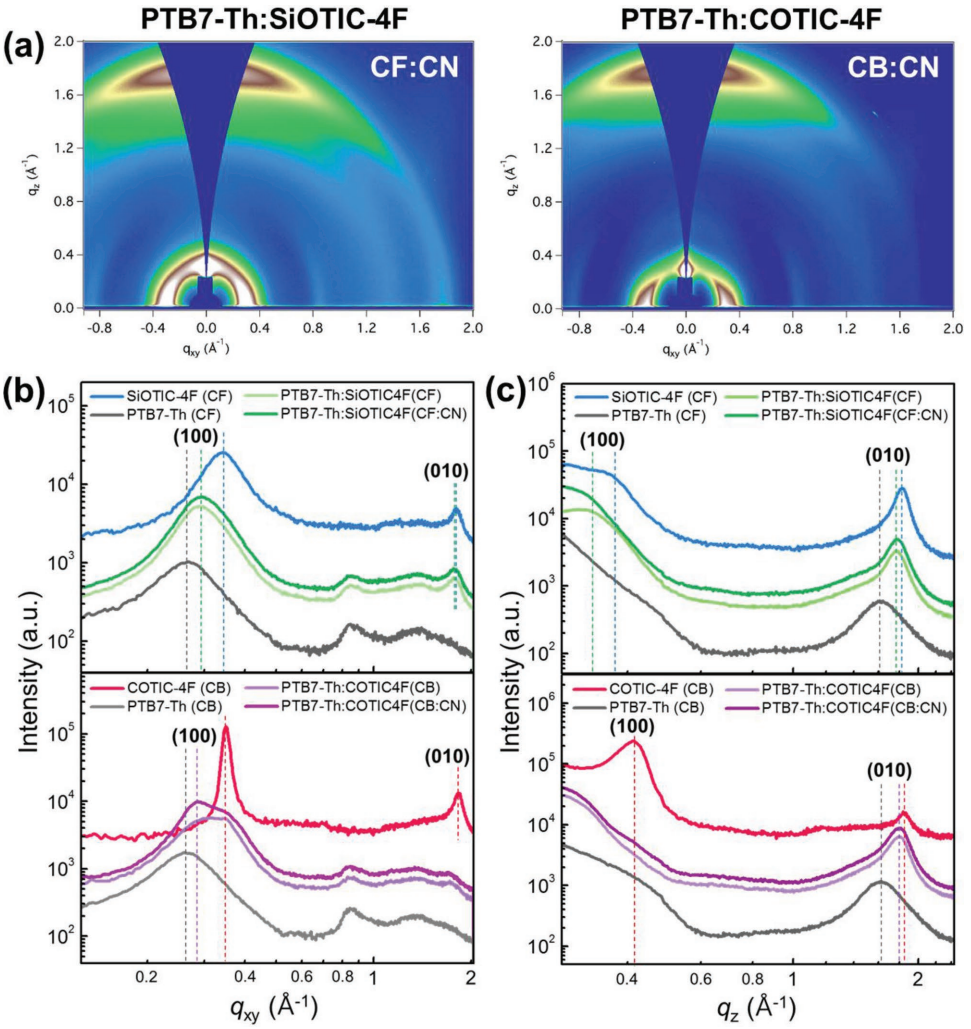

Figure 4. a) 2D GIWAXS images for optimized blend films. b) In-plane and c) out-of-plane line-cut profiles for neat and blend films.

peak (010) located at q_z = 1.82 Å^{-1}. The (010) diffractions of NFA neat films along the out-of-plan direction correspond to a π–π stacking distance of ≈3.4 Å, which is smaller than that of the as-spun PTB7-Th (≈3.8 Å). The optimized blend films for both NFAs show a preferential face-on orientation (**Figure 4**a), which is beneficial for efficient charge transport in the vertical direction between the electrodes.[42] In both NFA blends, the inter-lamellae (100) region in the in-plane direction and π–π stacking (010) region in the out-of-plane direction contain features from the PTB7-Th and NFA components that cannot be easily separated. We speculate that the donor and acceptor components maintain their crystalline features,[43,44] as well as part of the components being reorganized into mixed phases in the BHJ blends. The (010) crystal coherence lengths (L_C) for face-on crystals are estimated to be 33.5 and 29.0 nm for the SiOTIC-4F:PTB7-Th and COTIC-4F:PTB7-Th blend films, respectively. Overall, a combination of morphology characterization results based on TEM, GIWAXS, and SCLC mobility data indicates that both NFAs have quite similar film properties.

In conclusion, we describe the synthesis and characterization of two novel and simple methods to prepare NBG small molecule NFAs for the fabrication of efficient near-infrared OSCs. SiOTIC-4F-based cells show a high PCE of 9.0% with a J_{SC} as high as ≈22.8 mA cm^{-2}. The EQE spectrum indicates strong light harvesting across the broad solar spectrum and efficient hole/electron transfer between PTB7-Th and SiOTIC-4F, leading to a high J_{SC}. Of particular relevance is the small energy loss of ≈0.52 eV and a good AVT of 53.4% in the blends with PTB7-Th, suggesting the great potential of NIR small molecular acceptors in the field of semitransparent OSCs. The simplicity of preparation, wide range of possible structural modifications, tendencies to provide appropriate morphological organizations, and ability to generate current under enthalpically challenged conditions suggest that a wide range of additional NFAs can be further designed based on the molecular framework illustrated by SiOTIC-4F and COTIC-4F.

Supporting Information

Supporting Information is available from the Wiley Online Library or from the author.

Acknowledgements

J.L. and S.-J.K. contributed equally to this work. This work was supported by the Office of Naval Research (N00014-14-1-0580) and the Center for Advanced Soft-Electronics funded by the Ministry of Science and ICT as Global Frontier Project (Code No. 2011–0031628). Work at the Molecular Foundry was supported by the Office of Science, Office of Basic Energy Sciences, of the U.S. Department of Energy under Contract No. DE-AC02-05CH11231. The authors are grateful to the Pohang Accelerator Laboratory for providing the synchrotron radiation sources at 9A beamline. The authors would like to acknowledge Dr. Karen Bustillo for her assistance with TEM measurements.

Conflict of Interest

The authors declare no conflict of interest.

Keywords

near-infrared optoelectronics, non-fullerene acceptors, organic solar cells

Received: April 23, 2018
Revised: May 19, 2018
Published online: June 28, 2018

[1] C. J. Traverse, R. Pandey, M. C. Barr, R. R. Lunt, *Nat. Energy* **2017**, *2*, 849.
[2] C. J. M. Emmott, J. A. Rohr, M. Campoy-Quiles, T. Kirchartz, A. Urbina, N. J. Ekins-Daukes, J. Nelson, *Energy Environ. Sci.* **2015**, *8*, 1317.
[3] R. R. Lunt, V. Bulovic, *Appl. Phys. Lett.* **2011**, *98*, 113305.
[4] L. T. Dou, Y. S. Liu, Z. R. Hong, G. Li, Y. Yang, *Chem. Rev.* **2015**, *115*, 12633.
[5] J. Yuan, M. Ford, G. Ding, H. Dong, M. Wang, L. Han, Y. Li, G. C. Bazan, W. Ma, *J. Mater. Chem. A* **2016**, *4*, 17333.
[6] L. Ying, F. Huang, G. C. Bazan, *Nat. Commun.* **2017**, *8*, 14047.
[7] C. Liu, K. Wang, X. Gong, A. J. Heeger, *Chem. Soc. Rev.* **2016**, *45*, 4825.
[8] L. Ying, B. B. Y. Hsu, H. Zhan, G. C. Welch, P. Zalar, L. A. Perez, E. J. Kramer, T.-Q. Nguyen, A. J. Heeger, W.-Y. Wong, G. C. Bazan, *J. Am. Chem. Soc.* **2011**, *133*, 18538.
[9] W. Li, K. H. Hendriks, A. Furlan, M. M. Wienk, R. A. J. Janssen, *J. Am. Chem. Soc.* **2015**, *137*, 2231.
[10] D. Baran, T. Kirchartz, S. Wheeler, S. Dimitrov, M. Abdelsamie, J. Gorman, R. S. Ashraf, S. Holliday, A. Wadsworth, N. Gasparini, P. Kaienburg, H. Yan, A. Amassian, C. J. Brabec, J. R. Durrant, I. McCulloch, *Energy Environ. Sci.* **2016**, *9*, 3783.
[11] Z. He, B. Xiao, F. Liu, H. Wu, Y. Yang, S. Xiao, C. Wang, T. P. Russell, Y. Cao, *Nat. Photonics* **2015**, *9*, 174.
[12] D. D. Nuzzo, G.-J. A. H. Wetzelaer, R. K. M. Bouwer, V. S. Gevaerts, S. C. J. Meskers, J. C. Hummelen, P. W. M. Blom, R. A. J. Janssen, *Adv. Energy Mater.* **2013**, *3*, 85.
[13] Y. Li, J.-D. Lin, X. Che, Y. Qu, F. Liu, L.-S. Liao, S. R. Forrest, *J. Am. Chem. Soc.* **2017**, *139*, 17114.
[14] W. Wang, C. Yan, T.-K. Lau, J. Wang, K. Liu, Y. Fan, X. Lu, X. Zhan, *Adv. Mater.* **2017**, 1701308.
[15] Y. Cui, C. Yang, H. Yao, J. Zhu, Y. Wang, G. Jia, F. Gao, J. Hou, *Adv. Mater.* **2017**, *29*, 1703080.
[16] Z. Xiao, X. Jia, D. Li, S. Wang, X. Geng, F. Liu, J. Chen, S. Yang, T. P. Russell, L. Ding, *Sci. Bull.* **2017**, *62*, 1494.
[17] J. Sun, X. Ma, Z. Zhang, J. Yu, J. Zhou, X. Yin, L. Yang, R. Geng, R. Zhu, F. Zhang, W. Tang, *Adv. Mater.* **2018**, 1707150.
[18] Z. Yao, X. Liao, K. Gao, F. Lin, X. Xu, X. Shi, L. Zuo, F. Liu, Y. Chen, A. K.-Y. Jen, *J. Am. Chem. Soc.* **2018**, *140*, 2054.
[19] J. Hou, O. Inganäs, R. H. Friend, F. Gao, *Nat. Mater.* **2018**, *17*, 119.
[20] G. Zhang, J. Zhao, P. C. Y. Chow, K. Jiang, J. Zhang, Z. Zhu, J. Zhang, F. Huang, H. Yan, *Chem. Rev.* **2018**, *118*, 3447.
[21] T. Ameri, G. Dennler, C. Waldauf, H. Azimi, A. Seemann, K. Forberich, J. Hauch, M. Scharber, K. Hingerl, C. J. Brabec, *Adv. Funct. Mater.* **2010**, *20*, 1592.
[22] Y. Li, X. Liu, F.-P. Wu, Y. Zhou, Z.-Q. Jiang, B. Song, Y. Xia, Z.-G. Zhang, F. Gao, O. Inganäs, Y. Li, L.-S. Liao, *J. Mater. Chem. A* **2016**, *4*, 5890.
[23] Y. Li, L. Zhong, B. Gautam, H.-J. Bin, J.-D. Lin, F.-P. Wu, Z. Zhang, Z.-Q. Jiang, Z.-G. Zhang, K. Gundogdu, Y. Li, L.-S. Liao, *Energy Environ. Sci.* **2017**, *10*, 1610.
[24] J. Liu, S. Chen, D. Qian, B. Gautam, G. Yang, J. Zhao, J. Bergqvist, F. Zhang, W. Ma, H. Ade, O. Inganäs, K. Gundogdu, F. Gao, H. Yan, *Nat. Energy* **2016**, *1*, 16089.
[25] Y. J. Cheng, S. H. Yang, C. S. Hsu, *Chem. Rev.* **2009**, *109*, 5868.
[26] J. E. Coughlin, A. Zhugayevych, R. C. Bakus, T. S. van der Poll, G. C. Welch, S. J. Teat, G. C. Bazan, S. Tretiak, *J. Phys. Chem. C* **2014**, *118*, 15610.
[27] H. Huang, L. Yang, A. Facchetti, T. J. Marks, *Chem. Rev.* **2017**, *117*, 10291.
[28] N. E. Jackson, B. M. Savoie, K. L. Kohlstedt, M. Olvera de la Cruz, G. C. Schatz, L. X. Chen, M. A. Ratner, *J. Am. Chem. Soc.* **2013**, *135*, 10475.
[29] W. Zhao, S. Li, H. Yao, S. Zhang, Y. Zhang, B. Yang, J. Hou, *J. Am. Chem. Soc.* **2017**, *139*, 7148.
[30] S. Dai, F. Zhao, Q. Zhang, T.-K. Lau, T. Li, K. Liu, Q. Ling, C. Wang, C. Lu, W. You, X. Zhan, *J. Am. Chem. Soc.* **2017**, *139*, 1336.
[31] C. M. Cardona, W. Li, A. E. Kaifer, D. Stockdale, G. C. Bazan, *Adv. Mater.* **2011**, *23*, 2367.
[32] C. J. Takacs, Y. Sun, G. C. Welch, L. A. Perez, X. Liu, W. Wen, G. C. Bazan, A. J. Heeger, *J. Am. Chem. Soc.* **2012**, *134*, 16597.
[33] G. C. Welch, R. C. Bakus, S. J. Teat, G. C. Bazan, *J. Am. Chem. Soc.* **2013**, *135*, 2298.
[34] N. D. Eisenmenger, G. M. Su, G. C. Welch, C. J. Takacs, G. C. Bazan, E. J. Kramer, M. L. Chabinyc, *Chem. Mater.* **2013**, *25*, 1688.
[35] R. C. Coffin, J. Peet, J. Rogers, G. C. Bazan, *Nat. Chem.* **2009**, *1*, 657.
[36] J. Ku, Y. Gim, Y. Lansac, Y. H. Jang, *Phys. Chem. Chem. Phys.* **2016**, *18*, 1017.
[37] L. Zhang, M. Yu, H. Zhao, Y. Wang, J. Gao, *Chem. Phys. Lett.* **2013**, *570*, 153.
[38] C. J. Takacs, S. D. Collins, J. A. Love, A. A. Mikhailovsky, G. C. Bazan, T.-Q. Nguyen, A. J. Heeger, *ACS Nano* **2014**, *8*, 8141.
[39] C. Groves, O. G. Reid, D. S. Ginger, *Acc. Chem. Res.* **2010**, *43*, 612.
[40] M. Guide, X.-D. Dang, T.-Q. Nguyen, *Adv. Mater.* **2011**, *23*, 2313.
[41] V. Vohra, K. Kawashima, T. Kakara, T. Koganezawa, I. Osaka, K. Takimiya, H. Murata, *Nat. Photonics* **2015**, *9*, 403.
[42] J. Lee, D. H. Sin, B. Moon, J. Shin, H. G. Kim, M. Kim, K. Cho, *Energy Environ. Sci.* **2017**, *10*, 247.
[43] S. Chen, Y. Liu, L. Zhang, P. C. Y. Chow, Z. Wang, G. Zhang, W. Ma, H. Yan, *J. Am. Chem. Soc.* **2017**, *139*, 6298.
[44] F. Liu, Z. Zhou, C. Zhang, T. Vergote, H. Fan, F. Liu, X. Zhu, *J. Am. Chem. Soc.* **2016**, *138*, 15523.

